

https://doi.org/10.1070/QEL17963

Melanin diagnostics with nonlinear optics: a mini-review

E.A. Shirshin, B.P. Yakimov, G.S. Budylin, K.E. Buyankin,
A.G. Armaganov, V.V. Fadeev, A.A. Kamalov

Abstract. **Optical methods are widely used to perform fundamental studies of living systems and solve problems of biomedical diagnostics. Along with the classical spectroscopy, methods of nonlinear optics (e.g., multiphoton microscopy) are also applied in biophotonics. The potential of nonlinear optical methods for visualisation and analysis of the properties of endogenous chromophore molecules are considered in this minireview. Melanin – a pigment with specific spectral features of photophysical properties in the visible and near-IR ranges – is taken as an example. It is discussed what information about its localisation in tissues and structural organisation can be obtained by nonlinear optical methods: multiphoton fluorescence microscopy (including fluorescence lifetime imaging), third harmonic generation, pump–probe spectroscopy, and coherent anti-Stokes Raman spectroscopy.**

Keywords: *melanin, nonlinear processes, multiquantum processes, multiphoton microscopy, visualisation of fluorescence decay time, FLIM, CARS, pump–probe spectroscopy.*

1. Introduction

Methods of optical spectroscopy and microscopy are widely used in both fundamental biophysical and applied biomedical studies. Possessing a molecular specificity, optical spectroscopy allows one to study changes in the macromolecular structure; characterise intermolecular interactions; and analyse complex systems: biofluids, cells, or tissues. Typical biomedical applications of optical spectroscopy are point-of-care diagnostics (for example, saliva-based rapid tests for COVID-19 [1]) and intraoperative diagnostics (e.g., in endocrinology and urology) [2]. Optical microscopy, in turn, makes it possible to visualise biochemical processes and structure of biological objects with almost submicron (i.e., subcellular) resolution [3]. Thus, the combination of optical microscopy and spectroscopy methods is a highly efficient tool for studying living systems.

For some natural reasons (in particular, simplicity and low cost), 'linear' optical methods that use electromagnetic fields of low strength have become more popular in biomedical diagnostics. These methods include Raman spectroscopy; absorption and reflection spectroscopy in visible and IR spectral ranges; and fluorescence spectroscopy, in particular, time-resolved spectroscopy. Among the nonlinear optical methods, the most popular one appears to be the multiphoton microscopy (MPM), which implies measurement of two- and three-photon fluorescence and second- and third-harmonic generation (SHG, THG) signals [3]. This popularity is explained by the increased sample scanning depth (due to the shift of excitation wavelength to the transparency window of biological tissues), reduced photodamage, and increased spatial resolution. At the same time, the results of some studies demonstrate unique possibilities of biomedical diagnostics open due to the use of other nonlinear optical methods, e.g., stimulated Raman scattering (SRS), coherent anti-Stokes scattering (CARS), and the pump–probe method. The purpose of this minireview is to reveal the parameters of systems studied that could be measured using nonlinear optical methods in biophotonics. Here, we will consider melanin as a object of study. This is a pigment determining the color of skin, hair, and eyes, which is involved in a number of pathological processes in organism [4]; it is also used to prepare various nanomaterials [5]. Then we will discuss what information about the structure, properties, and localisation of melanin in organism can be obtained by applying an arsenal of optical methods.

Melanin was chosen by us not only in view of its importance in biology and medicine but also because of its unusual spectral properties, primarily, the absorption ones [6, 7]. In contrast to standard chromophores, whose absorption spectra contain bell-shaped bands (due to electronic–vibrational transitions), the absorption spectrum of melanin has no pronounced features and presents a curve monotonically decreasing with increasing wavelengths from the visible to near-IR spectral region. In the range of 300–1000 nm the dependence

E.A. Shirshin, K.E. Buyankin Faculty of Physics, Lomonosov Moscow State University, Leninskie Gory 1, stroenie 2, 119991 Moscow, Russia; Medical Research and Educational Center, Lomonosov Moscow State University, Lomonosovskii prosp. 27, korp. 10, 119192 Moscow, Russia; e-mail: shirshin@lid.phys.msu.ru;
B.P. Yakimov Faculty of Physics, Lomonosov Moscow State University, Leninskie Gory 1, stroenie 2, 119991 Moscow, Russia; Medical Research and Educational Center, Lomonosov Moscow State University, Lomonosovskii prosp. 27, korp. 10, 119192 Moscow, Russia; World-Class Research Center "Digital Biodesign and Personalised Healthcare", I.M. Sechenov First Moscow State Medical University (Sechenov University), Ministry of Health of the Russian Federation, ul. Trubetskaya 8, stroenie 2, 119991 Moscow, Russia;
G.S. Budylin World-Class Research Center "Digital Biodesign and Personalised Healthcare", I.M. Sechenov First Moscow State Medical University (Sechenov University), Ministry of Health of the Russian Federation, ul. Trubetskaya 8, stroenie 2, 119991 Moscow, Russia; Institute of Spectroscopy, Russian Academy of Sciences, ul. Fizicheskaya 5, Troitsk, 108840 Moscow, Russia;
V.V. Fadeev Faculty of Physics, Lomonosov Moscow State University, Leninskie Gory 1, stroenie 2, Moscow, 119991 Russia;
A.G. Armaganov, A.A. Kamalov Medical Research and Educational Center, Lomonosov Moscow State University, Lomonosovskii prosp. 27, korp. 10, 119192 Moscow, Russia

Received 21 October 2021
Kvantovaya Elektronika **52** (1) 28–35 (2022)
Translated by Yu.P. Sin'kov

of melanin absorptance A on the wavelength λ can be described by an exponential law: $A \sim \exp(-\lambda/\Lambda)$, where Λ is the slope of the absorption curve on the semilogarithmic scale. This parameter, both for synthetic and natural melanins and for different melanin forms, may vary approximately from 80 to 160 nm. The existence of absorption in the IR region and the specific features of the photophysical processes occurring in melanin (see Section 2) make this substance interesting for study by optical methods, including nonlinear ones. Section 3 contains examples of application of nonlinear optical methods (MPM, CARS, SRS, pump–probe) for analysis of melanin in different systems and some conclusions about the information on a biosystem studied, provided by each of these methods.

2. Optical properties of melanin: nonstandard chromophore

2.1. Specificity of the spectral properties of melanin

Melanin is a pigment, i.e., a mixture of different compounds, formed in organism as a result of oxidation of precursor molecules [4]. Depending on the chemical composition, one can select different melanin subtypes with different properties, including optical ones; these are eumelanin, pheomelanin, neuromelanin, and pyomelanin [8]. For example, the difference between eumelanin and pheomelanin, which dominate in skin, is as follows: eumelanin consists mainly of nitrogen-containing indoles, whereas pheomelanin consists of benzothiazines and benzothiazones, containing sulphur atoms. Since different melanin subtypes have similar optical properties, we will not differentiate them rigorously. The spectral characteristics of melanin differs significantly from those of other chromophores: it has a wide 'exponential' absorption spectrum; its fluorescence can be excited in a wide wavelength range, including the IR region [9]; and its fluorescence decay kinetics contains an ultrafast component (~1 ps) [10], which is due to the high nonradiative relaxation rate of the excited state [11].

The mechanism of the formation of melanin spectral properties is still debated. For example, a model describing the formation of the melanin absorption spectrum in terms of exciton interaction in disordered aggregates of molecular structures was proposed in [6]. It is assumed in this model that melanin synthesis may give rise to different structural units (oligomers), which then interact with each other. Electron interaction leads to spectral shifts and broadening, and the intensity of this interaction depends on the distance between oligomers and mutual orientation of their dipole moments.

Since the spectral properties of melanin differ significantly from those of other skin chromophores, researchers have tried to solve the problem of quantitative analysis of melanin using all available spectral methods. Primarily, the interest in melanin is related to the diagnostics of melanoma – the most dangerous skin cancer [12]. In particular, the following methods were applied to study melanin *in vivo* directly in skin:

(1) Diffuse reflectance spectroscopy (Fig. 1, panel 1) [13, 14]. The presence of melanin in skin determines its colour and, correspondingly, the absorption and reflection spectra. Since the melanin spectrum differs significantly from those of other main skin chromophores, its contribution to the formation of reflected optical signal in the visible and near-IR regions can be determined unambiguously. This approach is applied also to estimate the sun protection factor (SPF) [15] and choose the appropriate radiation dose when irradiating skin [16].

(2) Fluorescence spectroscopy of melanin in the near-IR range upon excitation in the red and IR regions (Fig. 1, panel 2) [17, 18]. The presence of a long-wavelength tail in the absorption spectrum of melanin makes it possible to implement its direct single-photon excitation, leading to emission in the IR spectral region. For example, at an excitation wavelength of 785 nm, which is often used in Raman spectroscopy of biological tissues, the skin melanin is responsible for the wide fluorescent background in the range of 900–1000 nm, which obscures partially weak vibrational bands [19]. The human organism does not contain (in the first approximation) any other endogenous fluorophores active in this spectral region, due to which the red and IR fluorescence of melanin can be used for its diagnostics [20–22].

(3) Optoacoustic detection (Fig. 1, panel 3). Since melanin can absorb light in the near-IR spectral range, it can be detected using optoacoustic methods: its selective absorption of pulsed pump radiation leads to local heating, accompanied by generation of an acoustic signal; the temporal profile of the latter allows one to localise melanin over tissue depth. In addition, optoacoustic detection of melanin was used to implement *in vivo* flow cytometry: when exposing vessels to 1064-nm light, an optoacoustic signal generated by single cells (melanocytes) was detected. Thus, a sensitivity sufficient for detecting *in vivo* single melanocytes in blood flow was achieved [23], which can be used to detect metastases in patients with melanoma.

(4) Raman spectroscopy and microspectroscopy. The heterogeneity of molecular composition and structural organisation of melanin determines its characteristic Raman spectrum. In particular, the spectrum of the most widespread form of melanin – eumelanin – contains bands in the range of 1000–1800 cm^{-1} at the following frequencies: 1220 cm^{-1} (C–OH and C–O stretching vibrations of phenol and carboxyl groups, respectively), 1340 cm^{-1} (C–N indole vibrations), and 1390 cm^{-1} (vibrations in aromatic C=C fragments; the A_{1g} symmetry is similar to that of the D band in disordered graphite), as well as bands at frequencies of 1562 and 1598 cm^{-1}, which are due to the C=C vibrations of sp2-hybridised carbon and C–C indole vibrations (E_{2g} symmetry) [24–26]. In view of the heterogeneity of molecular composition and environment, the aforementioned bands merge into two wide bands, peaking approximately at ~1380 and ~1570 cm^{-1}, with half-widths of ~200 and 150 cm^{-1}, respectively. The amplitudes and positions of these bands may vary, depending on the excitation wavelength, chemical composition, and structural organisation, which makes it possible to analyse melanin both *in vitro* [27] and *in vivo* [18]. For example, skin spectra with a depth resolution of 2 μm were recorded in [19] using Raman microspectroscopy, and the melanin contribution was selected in them. It was found that the skin IR fluorescence intensity correlates with the amplitude of melanin contribution to the Raman spectrum; the melanin depth distribution in skin, including the surface (horny) layer, was also determined. The skin structure and melanin localisation domains in skin are schematically shown in Fig. 2a. Residues of melanin particles (melanosomes) can be observed in the horny layer; their concentration and size increase with an increase in the epidermis depth. At the interface between the living epidermis and papillary dermis, in the localisation domain of melanin-synthesising cells (melanocytes), the melanin concentration has a local maximum. The Raman spec-

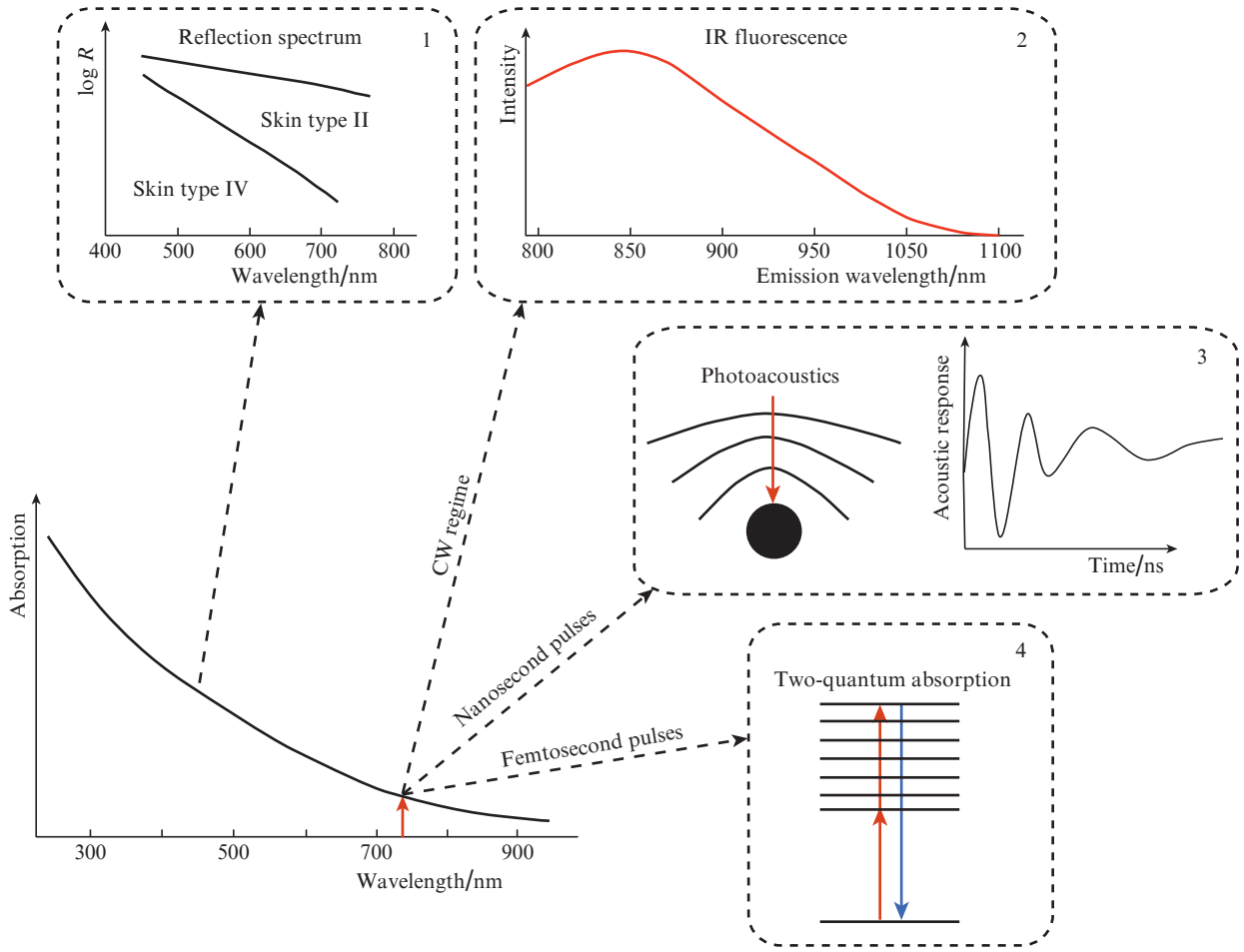

Figure 1. (Colour online) Specific features of the optical properties of melanin: absorption spectra of melanin in the visible and near-IR ranges and schematics of the optical methods based on the use of the long-wavelength absorption tail of melanin.

trum of eumelanin, measured *in vivo* in skin, is shown in Fig. 2b. Other melanin forms also exhibit wide Raman bands: for example, pheomelanin (melanin subtype responsible for the red colour of hair) has three characteristic Raman bands at frequencies of 500, 1440, and 2000 cm^{-1} [28].

Thus, melanin can be successfully detected by methods of classical spectroscopy and microscopy; this approach is based on the specificity of its spectral properties. At the same time, the possibilities of optical diagnostics of the melanin structure and properties can be significantly expanded due to the use of nonlinear optical methods.

3. Application of nonlinear optical methods for studying the structure and properties of melanin and its localisation in human body

3.1. Multiphoton fluorescence and fluorescence lifetime imaging for *in vivo* diagnostics of skin melanin

3.1.1 On the mechanism of melanin fluorescence excitation in the visible region: two-photon or two-quantum absorption? Multiphoton microscopy has been actively used in biomedical diagnostics, since it has a number of advantages over conventional confocal microscopy. These advantages include large penetration depth in tissues (due to the pumping with a wavelength lying in the transparency window of biological tissues); less photodamage to the sample (the photochemical processes, the first stage of which is photon absorption, occur only in the beam waist); and the possibility of detecting not only fluorescence signal but also the signals of optical harmonic generation and fluorescence relaxation kinetics, which is achieved by conventional use of femtosecond laser pulses for pumping [3].

Fluorescence arises in MPM as a result of excitation of fluorophore molecules after the multiphoton absorption. Let us consider the case of two-photon absorption. In some studies melanin in skin was detected from its two-photon fluorescence signal (i.e., the fluorescence was excited in the IR spectral region, and the signal was recorded in the range of 400–500 nm), whose intensity greatly exceeds that of other endogenous fluorophores. Teuchner et al. paid attention to the fact that the fluorescence excitation in this case is most likely a two-quantum process rather than two-photon (Fig. 1, panel 4). The point is that melanin has real absorption in the region of IR excitation by pump radiation; therefore, the absorption of the second photon may occur via a real level rather than via a virtual one. The presence of a real level should lead to resonant enhancement of the third-order nonlinear susceptibility and increase in the two-photon absorption cross section. This question was discussed in a series of papers [30–32]. Experiments with different pump pulse durations were proposed to identify the excitation type: for longer pulses the probability of two-photon absorption should

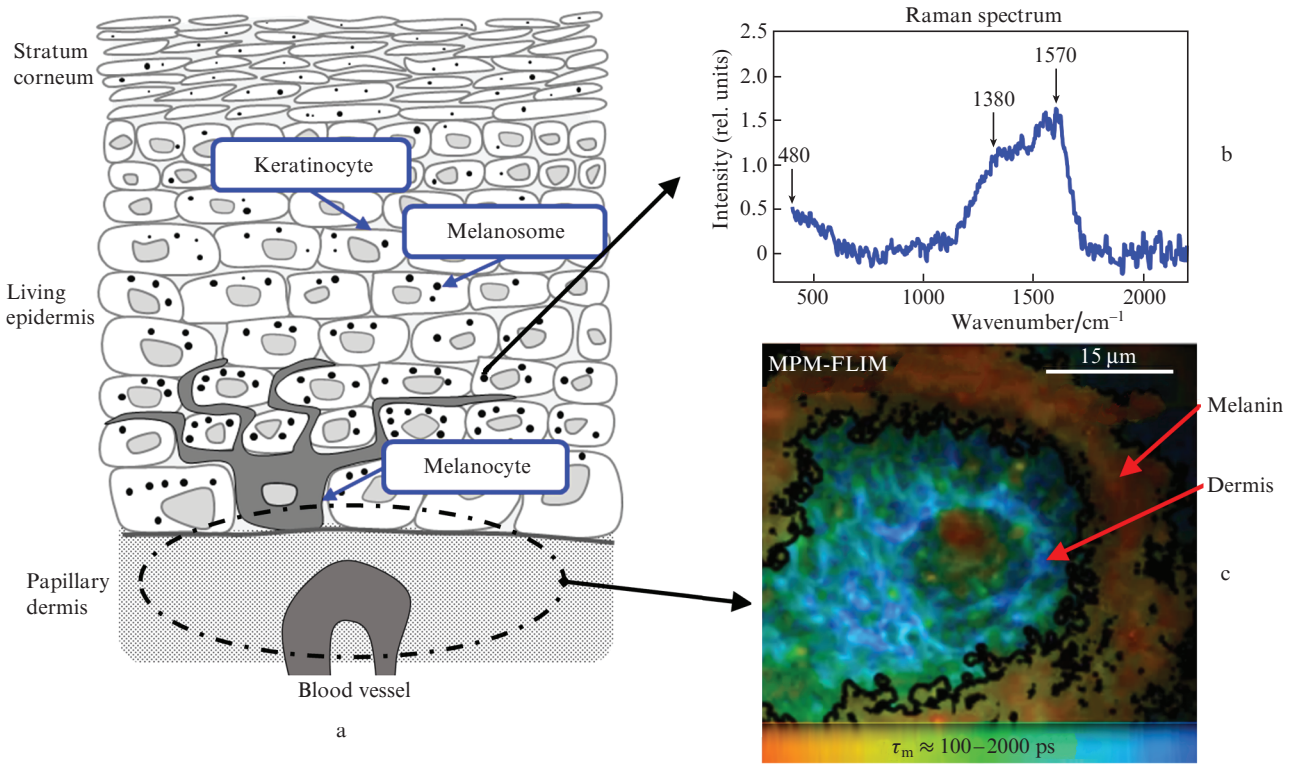

Figure 2. (Colour online) (a) Schematic image of the upper layers of skin structure and localisation of melanin in it; (b) Raman spectrum of skin, measured *in vivo* in the region of the basal cell layer (a characteristic feature of these Raman spectra is the presence of three wide lines near 500, 1380, and 1570 cm^{-1}, related to the Raman signal of eumelanin); (c) two-photon tomography (TPM-FLIM) image of skin in the region of basal layer [the average fluorescence lifetime is coded by colour; melanin exhibits fast fluorescence decay (orange colour), whereas the signal from collagen and elastin dermis fibres is characterised by a longer decay lifetime (blue colour)]. Panels (a) and (b) are adapted from [19], and panel (c) is adapted from [29].

decrease (because of the decrease in the photon fluence), and the process should shift towards two-step excitation [33]. It is of interest that two-photon fluorescence of melanin could be detected in a wide range of pump pulse durations: from femtoseconds [30] to nanoseconds [34]. Moreover, it was stated in [35] that multiphoton fluorescence of melanin can also be excited using continuous wave (cw) pumping.

3.1.2 MPM for melanin visualisation in skin. Independent of the mechanism of two-photon excitation of fluorescence of melanin, an undoubted fact is that MPM and, in particular, TPM fit excellently for its visualisation. There are three favourable factors:

(1) Fluorescence of melanin in skin can be excited selectively, for example at a wavelength of 800 nm. This wavelength falls in the minimum of excitation spectrum of the main endogenous cellular fluorophore, NAD(P)H; therefore, the melanin fluorescence dominates in detected signal [36–38].

(2) Even with shorter multiphoton excitation wavelengths, falling in the absorption maximum for other skin fluorophores, for example, NAD(P)H (700–750 nm), melanin fluorescence under conditions of confocal detection in the basal layer is several several times higher than the signal from other skin structures [29].

(3) The melanin fluorescence decay is ultrafast; i.e., it is shorter than the characteristic width of instrumental function in fluorescence lifetime imaging microscopy (FLIM) measurements (several tens of picoseconds) [39, 40].

Let us consider the above factors by an example of measuring the characteristics of healthy volunteer skin using MPM-FLIM with the excitation wavelength of 760 nm (Dermalnspect, JenLab). Figure 2c presents an image obtained in [29] by the TPM method for healthy volunteer skin. This is a typical fluorescent image of the basal skin layer, obtained at a depth of 60 μm; the bright regions correspond to melanin, as confirmed by their fluorescence decay parameters (the melanin-containing regions are characterised by ultrafast fluorescence decay). The image in Fig. 2c was obtained by the FLIM method; i.e., the fluorescence decays were measured in each its pixel, and the average decay time of the excited state was found from the measured kinetics [3, 29]. Then the fluorescence decay time was coded by colour in the image: red and blue colours correspond to faster (~100 ps) and slower relaxation processes, respectively.

Note that the fluorescence signal from melanin in the basal layer generally exceeds the signal from other skin fluorophores (upon excitation at 760 nm the main fluorophore is the NAD(F)H molecule [41]). In the case of melanin it is difficult to speak in terms of concentration in view of the specificity of its molecular organisation; nevertheless, the presence of a long-wavelength tail in the absorption spectrum of melanin provides a contrast of its detection by the MPM-FLIM method not worse than by one order of magnitude.

3.2. Pump–probe microscopy for melanin structure analysis and melanoma diagnostics

Another way to visualise melanin and analyse its molecular organisation is the pump–probe method. Its essence is as follows: first, pump radiation puts the system in an excited state, after which (with some time delay) the system is exposed to

probe radiation; under these conditions, one can observe a change in the probe pulse absorption as compared with the absorption in an unexcited system. The concept of this approach to the analysis of melanin is based on the model of formation of its optical properties (specifically, the absorption spectrum).

As was indicated in some studies [6, 42–45], the long-wavelength structureless tail of melanin absorption is assumed to be partially due to the interaction between the melanin oligomers in pigment aggregates. Then one can suggest that, at different interactions between individual oligomers in nanoparticle aggregates, differences in the absorption spectra of the ground and excited states should be observed.

Similarly to the reasoning in [42, 44], we will consider the cases of 'ordered' and 'random' arrangements of oligomers. It was suggested in [42] that the observed absorption spectrum of melanin is a superposition of absorption lines whose spectral optical parameters (position of maximum, half-width, relative contribution) depend on the character of interaction. In the case of the ordered arrangement of oligomers, the efficiency of their electron interaction is higher, which should lead to broadening of the spectral absorption lines forming the spectrum. In contrast, the interaction between randomly arranged monomers is weaker, and the corresponding separate absorptions lines are narrower (Fig. 3a).

These suggestions can be verified using pump–probe spectroscopy with femtosecond temporal resolution. Let us consider a process in which a system is first exposed to radiation with a wavelength λ_1 and then to radiation with $\lambda_2 = \lambda_1 + \Delta\lambda$. If $\Delta\lambda$ is smaller than the characteristic width of melanin absorption line, which width is primarily determined by the oligomer interaction, after the absorption of radiation with λ_1 the radiation with λ_2 cannot be absorbed from the ground state, because the system is now excited. The so-called ground state bleaching (GSB) occurs, which manifests itself in a negative absorption amplitude for the probe radiation with the wavelength λ_2. If $\Delta\lambda$ exceeds the characteristic absorption spectral width of oligomer aggregates in the composition of melanin, the probe radiation with λ_2 will be absorbed by another oligomer aggregate, characterised by absorption at longer wavelengths. The typical probe-radiation absorption kinetics after the melanin exposure to pump radiation is shown in Figs 3b and 3c. Integer melanin particles exhibit intense interaction between individual molecular components, which leads to a pronounced negative response in the induced-absorption kinetics, related to the ground state bleaching (Fig. 3b), which is not observed for individual molecular fragments (Fig. 3c).

Thus, is was shown in a series of studies [43–47] how the kinetics of probe radiation absorption from the excited state can be used to investigate the melanin molecular organisa-

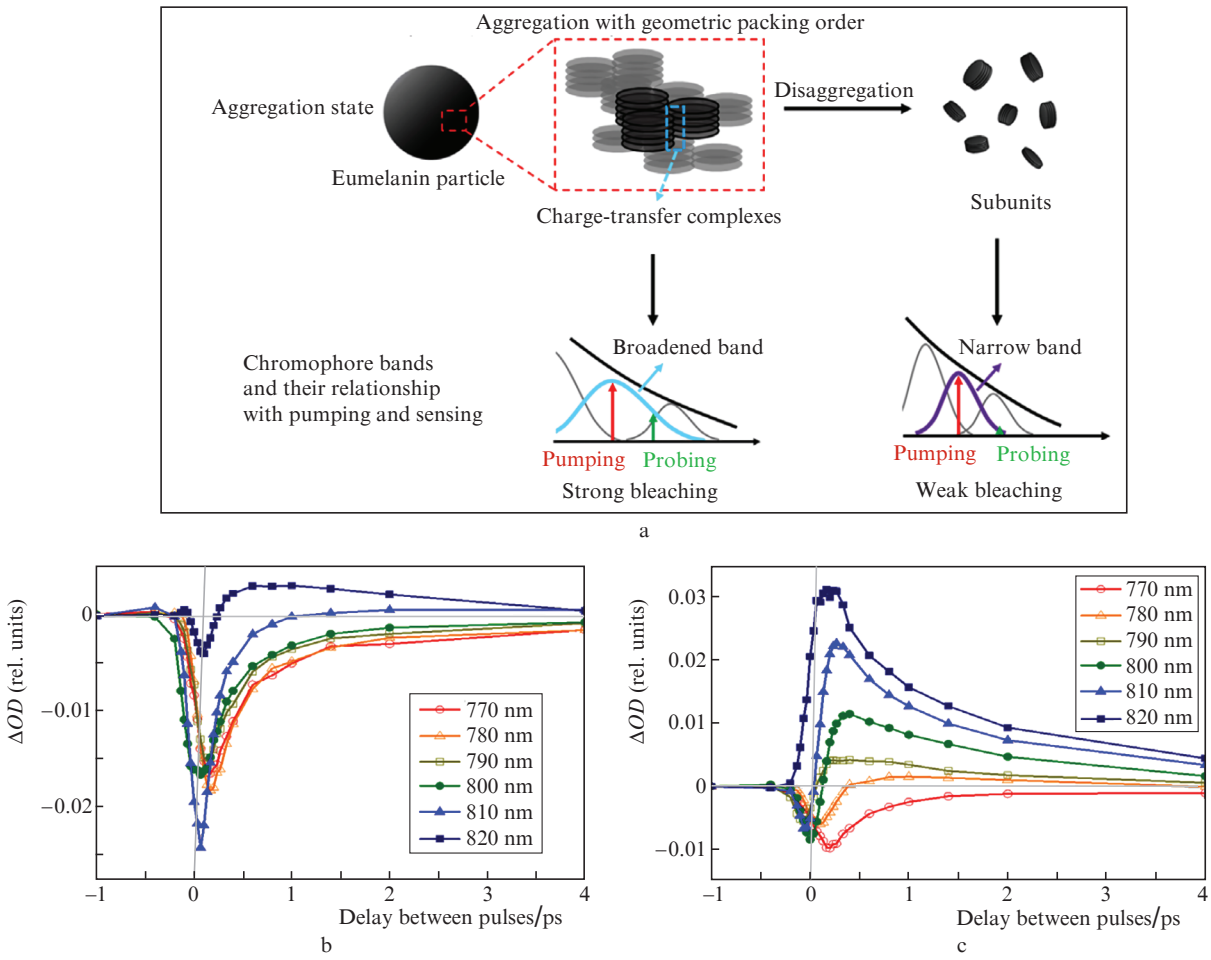

Figure 3. (Colour online) (a) Schematic of the formation of the melanin absorption spectrum and the induced-absorption kinetics (ΔOD) for different probe wavelengths at a pump wavelength of 700 nm, measured for (b) integer particles and (c) individual molecular melanin fragments, extracted from cuttlefish ink. Figure 3 is adapted from [46].

tion, which is not only of fundamental interest but also has direct practical significance, because the melanin molecular structure is related to the risk of melanoma metastasis [44]. In addition, the pump–probe technique makes it possible to separate melanin types, specifically, pheomelanin and eumelanin. The single-photon absorption spectra of both melanins are similar but have different temporal dynamics of their excited state, a circumstance lying in the basis of their selective visualisation by nonlinear optical methods [47].

3.3. SRS and CARS spectroscopy for melanin diagnostics

Methods of nonlinear vibrational spectroscopy – CARS and SRS – are also used to visualise melanin in tissues and perform selective mapping of eumelanin and pheomelanin.

The possibility of separating eumelanin and pheomelanin based on their Raman spectra was demonstrated by Gálvan et al. [26, 48], who showed on isolated melanin samples that eumelanin has three wide vibrational bands at 500, 1380, and 1580 cm^{-1}, whereas pheomelanin has bands at 500, 1490, and $\sim$2000 cm^{-1}; therefore, they can be distinguished in tissues.

As applied to visualisation problems, spontaneous Raman spectroscopy has some drawbacks. Primarily, spontaneous Raman scattering is characterised by a small interaction cross section; hence, the signal acquisition time is rather long, and one can hardly perform sample scanning in a reasonable time. In addition, a long-term irradiation of melanin may lead to its significant local heating and violate the pigment structure.

Alternatives for spontaneous Raman spectroscopy and microscopy are methods of nonlinear optics: CARS and SRS, which make it possible to analyse melanin with a much higher sensitivity. In these methods, two laser pulses with frequencies ω_p (pump beam) and ω_S (Stokes beam) are applied to the sample and the difference in the frequencies of the incident beams is chosen to match the vibrational frequency of interest: $\Omega = \omega_p - \omega_S$. In this case, vibrational modes are excited resonantly, and the efficiency of the vibrational frequency response can be increased by a factor of more than 10000 in comparison with the case of nonresonant spontaneous Raman scattering [49]. Due to this, one can map the distribution of molecules having isolated vibrational bands, e.g., lipids or proteins, with a high spatial resolution and a frame rate of 1–10 Hz. Biomedical visualisation is performed applying two main coherent Raman processes: CARS [50] and SRS [51, 52], which occur simultaneously. In the case of CARS, photons are generated at the anti-Stokes frequency, and an interaction of two photons (at the pump frequency ω_p and the Stokes frequency ω_S) occurs, so that radiation is detected at the frequency $\omega_{as} = \omega_p - \omega_S + \omega_p = \Omega + \omega_p$, which exceeds the pump frequency, and the resulting signal is free of noise caused by illumination (e.g., fluorescence) [53]. In the case of SRS, the signal is detected either at the frequency ω_S or at the frequency ω_p; the corresponding intensities change due to the stimulated emission from a virtual level formed as a result of excitation of molecule at the pump frequency.

To detect the pheomelanin response, it was proposed to use CARS microscopy with a pump frequency difference tuned to 2000 cm^{-1}, a frequency at which most of molecules have no pronounced vibrational bands, but strong Raman line of pheomelanin is observed. A possibility of detecting pheomelanin *in vivo* was demonstrated in [54]. CARS microscopy was also successfully applied to detect melanins in the case of the so-called amelanotic (i.e., having no pronounced color and pigmentation) form of melanoma.

Note that the intensity of the CARS signal generated by pheomelanin exceeds greatly the CARS intensity estimated from spontaneous Raman scattering cross sections. A possible explanation is the fact that the CARS signal is excited in the range of real absorption of melanin (the long-wavelength absorption tail in the near-IR range): in typical experiments the range of pump wavelengths at the Stokes component varies from 1040 to 1064 nm, and the pump wavelength lies in the range of 850–870 nm, which corresponds to the anti-Stokes component wavelength in the range of 718–735 nm. The presence of real absorption leads to resonant amplification of optical response [55]. Attempts have been made to introduce the CARS technique into clinical practice. For example, JenLab presented a CARS microscope as a component of a transportable platform with a mobile scanning unit, which can easily be brought to the desired part of a patient's body [56].

3.4. Method of third harmonic generation for analysis of melanin in cells

The THG method is widely used in nonlinear microscopy of cells and tissues. Because of the absence of phase matching in the bulk of medium, THG does not occur even under conditions of strong focusing; however, phase matching arises at the interface of two media with different refractive indices (as a result of changing the field phase), giving rise to significant THG [57]. Thus, using THG microscopy, one can perform efficient visualisation of interfaces between media with different refractive indices. The main range of SHG application in biophysics and biomedicine is the thorough analysis of collagen fibres [58]. Concerning THG, this technique is used for *in vivo* cytometry [59, 60], detection of lipid drops in cells [61], and neuroimaging [62]. Joint use of THG and SHG, which lies in the basis of the simultaneous label-free multiharmonic microscopy (SLAM) method, turned out to be fruitful for *ex vivo* optical biopsy [63]. As applied to melanin, THG is also used in some cases, related to the specificity of melanin photophysics.

It was shown in a number of studies that melanin is the most efficient THG source in skin. The THG for a model system – melanin hydrocolloids (particles of 100–200 nm diameter) – was investigated in [64]. It was established that the THG intensity depends linearly on the hydrocolloid concentration in solution; this was explained by the constructive interference from individual particles and the effect of incoherent hyper-Rayleigh scattering. The third-order nonlinear susceptibility $\chi^{(3)}$ was estimated to be three orders of magnitude higher than that of water. Further studies on cell cultures showed that the dependence of THG intensity on the melanin concentration (mass fraction (MF)) is described by a polynomial with an exponent of 3.5 at MF less than 11 mg mL^{-1} [65]. At the same time, at high melanin concentrations, this dependence becomes linear, which was explained in [65] by the transition from the resonant THG mode to the hyper-Rayleigh scattering of pump radiation by melanosomes inside the excited subfemtolitre volume. Afterwards THG visualisation was used in some studies for quantitative characterisation of melanin content *in vivo* and on histological sections [66, 67].

4. Conclusions

Methods of nonlinear optics provide additional information on the structural characteristics of the investigated system as compared with classical methods. In particular, in the case of melanin, this is information about its molecular organisation. Along with this, nonlinear optical methods allow one to implement visualisation with molecular contrast in tissues with higher sensitivity and resolution and at a larger depth, which was also demonstrated in this minireview by the example of melanin. Due to the development of elemental and instrumental base, nonlinear optical methods become increasingly popular in biomedical research. The aforementioned factors, as a whole, give grounds to expect progress in the field of clinical applications of nonlinear microscopy and spectroscopy in the nearest future.

Acknowledgements. This work was supported by the Russian Foundation for Basic Research (Grant No. 19-02-00947). The study was performed within the framework of the Development Programme 'Photonic and Quantum Technologies. Digital Medicine' for the Interdisciplinary Scientific and Educational School of Moscow University.

References

1. Wood B.R., Kochan K., Bedolla D.E., Salazar-Quiroz N., Grimley S.L., Perez-Guaita D., Baker M.J., Vongsvivut J., Tobin M.J., Bambery K.R., Christensen D., Pasricha S., Eden A.K., Mclean A., Roy S., Roberts J.A., Druce J., Williamson D.A., McAuley J., Catton M., Purcell D.F.J., Godfrey D.I., Heraud P. *Angewan. Chem. Internat. Edit*., **60**, 17102 (2021).
2. Solórzano C.C., Thomas G., Berber E., Wang T.S., Randolph G.W., Duh Q.Y., Triponez F. *Surgery*, **169**, 868 (2021).
3. Shirshin E.A., Yakimov B.P., Darvin M.E., Omelyanenko N.P., Rodionov S.A., Gurfinkel Y.I., Lademann J., Fadeev V.V., Priezzhev A.V. *Biochem. (Moscow)*, **84**, 69 (2019).
4. Simon J.D., Peles D., Wakamatsu K., Ito S. *Pigm. Cell Melanoma Resear*., **22**, 563 (2009).
5. Caldas M., Santos A.C., Veiga F., Rebelo R., Reis R.L., Correlo V.M. *Acta Biomater*., **105**, 26 (2020).
6. Chen C.-T., Chuang C., Cao J., Ball V., Ruch D., Buehler M.J. *Nat. Commun*., **5**, 1 (2014).
7. Micillo R., Panzella L., Iacomino M., Prampolini G., Cacelli I., Ferretti A., Crescenzi O., Koike K., Napolitano A., d'Ischia M. *Sci. Rep*., **7**, 1 (2017).
8. Cao W., Zhou X., McCallum N.C., Hu Z., Ni Q.Z., Kapoor U., Heil C.M., Cay K.S., Zand T., Mantanona A.J., Jayaraman A., Dhinojwala A., Deheyn D.D., Shawkey M.D., Burkart M.D., Rinehart J.D., Gianneschi N.C. *J. Am. Chem. Soc*., **143**, 2622 (2021).
9. Zonios G., Dimou A., Bassukas I., Galaris D., Tsolakidis A., Kaxiras E. *J. Biomed. Opt*., **13**, 014017 (2008).
10. Corani A., Pezzella A., Pascher T., Gustavsson T., Markovitsi D., Huijser A., d'Ischia M., Sundström V. *J. Phys. Chem. Lett*., **4**, 1383 (2013).
11. Kohl F.R., Grieco Ch., Kohler B. *Chem. Sci*., **11**, 1248 (2020).
12. Schadendorf D., Fisher D.E., Garbe C., Gershenwald J.E., Grob J.-J., Halpern A., Herlyn M., Marchetti M.A., McArthur G., Ribas A., Roesch A., Hauschild A. *Nat. Rev. Disease Prim*., **1**, 15003 (2015).
13. Zonios G., Bykowski J., Kollias N. *J. Investigat. Dermatol*., **117**, 1452 (2001).
14. Yudovsky D., Pilon L. *Appl. Opt*., **49**, 1707 (2010).
15. Throm C.M., Wiora G., Reble C., Schleusener J., Schanzer S., Karrer H., Kolbe L., Khazaka G., Meinke M.C., Lademann J. *J. Biophoton*., **14**, e202000348 (2021).
16. Dolotov L.E., Sinichkin Yu.P., Tuchin V.V., Utz S.R., Altshuler G.B., Yaroslavsky I.V. *Lasers Surg. Medic*., **34**, 127 (2004).
17. Huang Z., Zeng H., Hamzavi I., Alajlan A., Tan E., McLean D.I., Lui H. *J. Biomed. Opt*., **11**, 034010 (2006).
18. Huang Z., Lui H., Chen X.K., Alajlan A., McLean D.I., Zeng H. *J. Biomed. Opt*., **9**, 1198 (2004).
19. Yakimov B.P., Shirshin E.A., Schleusener J., Allenova A.S., Fadeev V.V., Darvin M.E. *Sci. Rep*., **10**, 14374 (2020).
20. Borisova E.G., Bratchenko I.A., Khristoforova Y.A., Bratchenko L.A., Genova T.I., Gisbrecht A.I., Moryatov A.A., Kozlov S.V., Troyanova P.P., Zakharov V.P. *Opt. Eng*., **59**, 1 (2020).
21. Bratchenko I.A., Artemyev D.N., Myakinin O.O., Khristoforova Y.A., Moryatov A.A., Kozlov S.V., Zakharov V.P. *J. Biomed. Opt*., **22** (2), 027005 (2017).
22. Khristoforova Y.A., Bratchenko I.A., Myakinin O.O., Artemyev D.N., Moryatov A.A., Orlov A.E., Kozlov S.V., Zakharov V.P. *J. Biophotonics*, **12**, e20180040 (2019).
23. Galanzha E.I., Menyaev Y.A., Yadem A.C., Sarimollaoglu M., Juratli M.A., Nedosekin D.A., Foster S.R., Jamshidi-Parsian A., Siegel E.R., Makhoul I., Hutchins L.F., Suen J.Y., Zharov V.P. *Sci. Translat. Med*., **11**, eaat5857 (2019).
24. Saha A., Arora R., Yakovlev V.V., Burke J.M. *J. Biophotonics*, **4**, 805 (2011).
25. Galván I., Jorge A., Solano F., Wakamatsu K. *Spectrochim. Acta Pt A: Molec. Biomolec. Spectros*., **110**, 55 (2013).
26. Galván I., Jorge A. *Ecol. Evolut*., **5**, 1425 (2015).
27. Kim Y.J., Wu W., Chun S.-E., Whitacre J.F., Bettinger C.J. *Proc. Nat. Acad. Sci*., **110**, 20912 (2013).
28. Galván I., Jorge A., Ito K., Tabuchi K., Solano F., Wakamatsu K. *Pigment Cell Melan. Res*., **26**, 917 (2013).
29. Shirshin E.A., Gurfinkel Y.I., Priezzhev A.V., Fadeev V.V., Lademann J., Darvin M.E. *Sci. Rep*., **7**, 1 (2017).
30. Teuchner K., Freyer W., Leupold D., Volkmer A., Birch D.J.S., Altmeyer P., Stucker M., Hoffmann K. *Photochem. Photobiol*., **70**, 146 (1999).
31. Teuchner K., Ehlert J., Freyer W., Leupold D., Altmeyer P., Stücker M., Hoffmann K. *J. Fluores*., **10** (3), 275 (2000).
32. Teuchner K., Mueller S., Freyer W., Leupold D., Altmeyer P., Stuecker M., Hoffmann K. *Multiphot. Absorp. Nonlin.Transmis. Proces.: Mater., Theory, Applicat*., **4797**, 211 (2003).
33. Gel'mukhanov F., Baev A., Ågren H., Macák P., Luo Y. *J. Opt. Soc. Am. B*, **19**, 937 (2002).
34. Eichhorn R., Wessler G., Scholz M., Leupold D., Stankovic G., Buder S., Stuecker M., Hoffmann K. *J. Biomed. Opt*., **14**, 034033 (2009).
35. Kerimo J., Rajadhyaksha M., DiMarzio C.A. *Photochem. Photobiol*., **87**, 1042 (2011).
36. Dimitrow E., Riemann I., Ehlers A., Koehler M.J., Norgauer J., Elsner P., König K., Kaatz M. *Experiment. Dermatol*., **18**, 509 (2009).
37. Sugata K., Sakai S., Noriaki N., Osanai O., Kitahara T., Takema Y. *Skin Resear. Technol*., **16**, 55 (2010).
38. Seidenari S., Arginelli F., Dunsby C., French P.M.W., König K., Magnoni C., Talbot C., Ponti G. *PLoS One*, **8**, e70682 (2013).
39. Seidenari S., Arginelli F., Bassoli S., Cautela J., French P.M.W., Guanti M., Guardoli D., König K., Talbot C., Dunsby C. *Dermatol. Res. Pract*., **2012**, 810749 (2012).
40. Dancik Y., Favre A., Loy C.J., Zvyagin A.V., Roberts M.S. *J. Biomed. Opt*., **18**, 1 (2013).
41. Koenig K., Riemann I. *J. Biomed. Opt*., **8**, 432 (2003).
42. Ju K.-Y., Degan S., Fischer M.C., Zhou K.C., Jia X., Yu J., Warren W.S. J. Biomed. Opt., 24 (5), 051414 (2019); https://doi.org/10.1117/1.JBO.24.5.051414.
43. Ju K.-Y., Fischer M.C., Warren W.S. *ACS Nano*, **12**, 12050 (2018).
44. Robles F.E., Deb S., Wilson J.W., Gainey C.S., Selim M.A., Mosca P.J., Tyler D.S., Fischer M.C., Warren W.S. *Biomed. Opt. Express*, **6**, 3631 (2015).
45. Simpson M.J., Wilson J.W., Robles F.E., Dall C.P., Glass K., Simon J.D., Warren W.S. *J. Phys. Chem. A*, **118**, 993 (2014).
46. Ju K.-Y., Degan S., Fischer M.C., Zhou K.C., Jia X., Yu J., Warren W.S. *J. Biomed. Opt*., **24**, 051414 (2019).
47. Robles F.E., Deb S., Vajzovic L., Vora G.K., Mruthyunjaya P., Warren W.S. *Translat. Vis. Sci. Technol*., **8**, 33 (2019).
48. Galván I., Jorge A., Ito K., Tabuchi K., Solano F., Wakamatsu K. *Pigment Cell Melan. Res*., **26**, 917 (2013).
49. Evans C. *Photochem. Photobiol*., **94** (4),624 (2018).

50. Ji-Xin C., Xie X.S. *J. Phys. Chem. B*, **108**, 827 (2003).
51. Freudiger C.W., Min W., Saar B.G., Lu S., Holtom G.R., He C., Tsai J.C., Kang J.X., Xie X.S. *Science*, **322**, 1857 (2008).
52. Hu F., Shi L., Min W. *Nature Meth*., **16**, 830 (2019).
53. Evans C.L., Xie X.S. *Ann. Rev. Analyt Chem*., **1**, 883 (2008).
54. Wang H., Osseiran S., Igras V., Nichols A.J., Roider E.M., Pruessner J., Tsao H., Fisher D.E., Evans C.L. *Sci. Rep*., **6**, 1 (2016).
55. Hudson B., Hetherington W., Cramer S., Chabay I., Klauminzer G.K. *Proc. Nat. Acad. Sci. USA*, **73**, 3798 (1976).
56. Weinigel M., Breunig H.G., König K. *Multiphot. Microscopy Biomed. Sci. XIV*, **8948**, 185 (2014).
57. Barad Y., Eisenberg H., Horowitz M., Silberberg Y. *Appl. Phys. Lett*., **70**, 922 (1998).
58. Chen X., Nadiarynkh O., Plotnikov S., Campagnola P.J. *Nat. Protocols*, **7**, 654 (2012).
59. Wu C.-H., Wang T.-D., Hsieh C.-H., Huang S.-H., Lin J.-W., Hsu S.-C., Wu H.-T., Wu Y.-M., Liu T.-M. *Sci. Rep*., **6**, 1 (2016).
60. Chen C.-K., Liu T.-M. *Biomed. Opt. Express*, **3**, 2860 (2012).
61. Débarre D., Supatto W., Pena A.-M., Fabre A., Tordjmann T., Combettes L., Schanne-Klein M.-C., Beaurepaire E. *Nat. Meth*., **3**, 47 (2005).
62. Lanin A.A., Pochechuev M.S., Chebotarev A.S., Kelmanson I.V., Bilan D.S., Kotova D.A., Tarabykin V.S., Ivanov A.A., Fedotov A.B., Belousov V.V., Zheltikov A.M. *Opt. Lett*., **45**, 836 (2020).
63. You S., Tu H., Chaney E.J., Sun Y., Zhao Y., Bower A.J., Liu Y.-Z., Marjanovic M., Sinha S., Pu Y., Boppart S.A. *Nat. Commun*., **9** (1), 1 (2018).
64. Su T.-Y., Liao C.-S., Yang C.-Y., Zhuo G.-Y., Chen S.-Y., Chu S.-W. *Appl. Phys. Lett*., **99**, 113702 (2011).
65. Sun C.-K., Liu W.-M., Liao Y.-H. *Biomed. Opt. Express*, **10**, 5716 (2019).
66. Liao Y.-H., Su Y.-H., Shih Y.-T., Chen W.-S., Jee S.-H., Sun C.-K. *J. Biomed. Opt*., **25**, 1 (2019).
67. Sun C.-K., Wu P.-J., Chen S.-T., Su Y.-H., Wei M.-L., Wang C.-Y., Gao H.-C., Sung K.-B., Liao Y.-H. *Biomed. Opt. Express*, **11**, 3009 (2020).